JOURNAL OF CATALYSIS 92, 98–108 (1985)

Studies on Iron–Manganese Oxide Carbon Monoxide Catalysts

I. Structure of Reduced Catalyst

K. B. JENSEN[1] AND F. E. MASSOTH[2]

Department of Fuels Engineering, University of Utah, Salt Lake City, Utah 84112

Received February 28, 1984; revised April 27, 1984

Iron–manganese catalysts have been found to show enhanced selectivity for low-molecular-weight olefins from synthesis gas. These catalysts have been investigated using a number of characterization techniques including: BET surface area, selective chemisorption, X-ray diffraction, electron microscopy, temperature-programmed desorption/reduction, electron spectroscopy for chemical analysis (ESCA), and infrared spectroscopy. The principle phases of the reduced catalysts were found to be α-iron and manganese(II) oxide, with the manganese oxide phase containing some iron(II) oxide in solid solution. A significant fraction of the iron was covered by the MnO phase, even at low Mn contents. Evidence was found for both associative and dissociative CO adsorption. A structural model of the reduced catalyst is proposed, which at low Mn contents consists of basic iron particles containing small platelets of Mn at the surface, while at high Mn levels it consists of a mixture of these and bulk MnO particles containing small amounts of Fe at their surface.

INTRODUCTION

Bulk iron catalysts promoted with manganese oxide have been reported to enhance the formation of low-molecular-weight olefins when used for carbon monoxide hydrogenation. Manganese oxide, among others, was mentioned by Bussemeir *et al.* (*1*) as a promoter for lower-molecular-weight olefins with iron-based catalysts. Kobel *et al.* (*2*) found high manganese content catalysts containing 10–20 wt% iron were also more selective to olefins. Yang (*3*) also reported manganese-promoted iron catalysts relatively more selective for low-molecular-weight olefins. Tsai (*4*) made a fixed-bed reactor study of precipitated iron catalysts promoted with various amounts of manganese and found enhanced olefin to paraffin selectivity for the catalysts moderately promoted with manganese. Recently, however, Van Dijk *et al.* (*5*) were unable to confirm increased olefin formation, though their reaction conditions were unclear. Also recently, Deckwer *et al.* (*6*) reported on the behavior of iron-manganese-based catalysts in the slurry phase and concluded that compared to the classical potassium-promoted iron precipitation catalysts, the iron-manganese catalysts gave higher yields of C_2 to C_4 olefins.

In order to gain insight into the manganese-promoted iron catalyst system, a characterization study of some precipitated iron–manganese catalysts was undertaken. The characterization tools used in this study included BET surface area, selective chemisorption, X-ray diffraction, electron microscopy, temperature-programmed desorption/reduction, ESCA, and infrared spectroscopy.

EXPERIMENTAL

Catalyst samples were the same as used in previous reaction studies (*4*). The catalysts had been prepared by adding an ap-

[1] Present address: Exxon Chemical Co., 4 Pearl Court, Allendale, N.J. 07401.

[2] To whom inquiries should be addressed.

0021-9517/85 $3.00

TABLE 1

Catalyst Compositions

Catalyst	Mn (at.%)	Catalyst	Mn (at.%)
C-0	0	C-29	29.1
C-1	1.1	C-39	38.7
C-2	2.1	C-52	52.2
C-3	3.1	C-74	73.5
C-5	5.3	C-86	85.9
C-15	15.0	C-100	100

propriate solution of iron and manganese nitrate to hot ammonium hydroxide. The precipitate was filtered, washed thoroughly, and then oven dried. Catalyst compositions as determined by X-ray fluorescence are listed in Table 1.

Pretreatment of the oven-dried catalyst consisted of a reduction with hydrogen at 500°C for 12 h, followed by passivation at room temperature by a controlled exposure to air. These catalysts could be activated by removing the surface oxide through a rereduction as required.

Helium was passed through commercial purifiers for oxygen and water removal; an extra precaution of a liquid-nitrogen trap was taken when warranted. Hydrogen was purified by passing through a Deoxo unit followed by molecular sieves. Carbon monoxide and premixed H_2/CO mixtures were passed through a trap containing active carbon and zeolite to remove possible carbonyl impurities. Other gases such as oxygen and carbon dioxide were rated at a purity of 99% or better and were used without further treatment.

A flow microbalance reactor was used to determine catalyst reduction profiles with temperature. X-Ray diffraction was performed on powdered catalyst samples with a Phillips instrument using Cu$K\alpha$ radiation. Surface areas were measured on a Micrometric BET Analyzer using N_2. A Hewlett–Packard spectrometer was used for the ESCA studies; passivated samples placed on double-stick Scotch tape were employed since provision for handling samples without exposure to air was not available. Photoacoustic spectroscopy (PAS) experiments were carried out on a specially modified Fourier Transform infrared spectrometric system (*7*). Samples were prereduced in a volumetric system, exposed to CO at 20 Torr for ½h, evacuated for 5 min, and transferred to a special PAS cell without exposure to air.

Chemisorption of various gases on reduced samples was measured in a conventional vacuum system. Carbon monoxide was used to estimate the specific surface area of iron. Initially, this was done by determining the carbon monoxide isotherm for the catalysts at room temperature and extrapolating the carbon monoxide chemisorbed at zero pressure from the desorption curve. Subsequent chemisorption measurements were made at −78°C using a double adsorption procedure. The specific iron surface area was estimated from the difference between the first and second adsorption of carbon monoxide at an arbitrary pressure of 300 Torr. Carbon dioxide and oxygen chemisorption values were determined at room temperature by extrapolating the desorption isotherm values to zero pressure.

Temperature-programmed desorption/reduction (TPD/TPR) were carried in a flow-tube reactor provided with a furnace and temperature programmer. Catalyst samples were reduced initially in hydrogen at 500°C overnight, purged with helium at the same temperature for about one-half hour and then cooled to room temperature. The catalysts were exposed to adsorbate gas at room temperature for one-half hour, flushed in helium for approximately 10 min, and then heated in a programmed schedule (10°C/min) in flowing helium or hydrogen. The off gases were monitored by a mass spectrometer scanning a mass range of 10–50 every 60 s. Flow rates were between 30 and 40 cm^3/min, and all experiments were performed at atmospheric pressure. The presence of 0.77% argon in the helium pro-

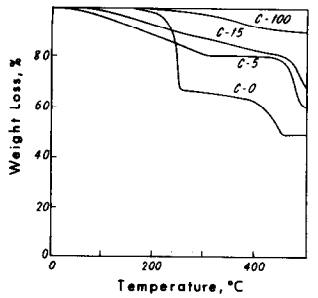

FIG. 1. Catalyst weight loss versus temperature during reduction. Numbers represent approximate at.% Mn in catalysts.

vided a marker peak in the mass spectra when this carrier gas was used.

The following sequence was employed in the TPD/TPR studies after initial reduction: Step 1—carbon monoxide was passed over the catalyst for one-half hour, flushed with helium, temperature programmed in helium to 500°C (TPD), and afterwards cooled; Step 2—at room temperature, the carrier gas was changed to hydrogen and the catalyst was temperature programmed in hydrogen (TPR); Step 3—after cooling in hydrogen again to room temperature, the catalyst was exposed to carbon monoxide for one-half hour. The catalyst was briefly flushed with hydrogen and then temperature programmed in hydrogen.

Further details on experimental procedures are given elsewhere (*8*).

RESULTS

A. Catalyst Reduction

Catalyst reduction was studied by observing the weight loss as the catalyst was reduced in hydrogen to 500°C. Weight loss results for several catalysts are given in Fig. 1. Relatively smooth reduction curves were obtained with essentially complete reduction being achieved within 1 h.

After reduction, the high iron content catalysts were dark in appearance. The high manganese catalysts were somewhat lighter and had a grey appearance. The pure manganese catalyst had a light green color but this quickly turned brown upon exposure to air. Some visual heterogeneity was observed in the high manganese catalysts, some catalyst particles being significantly lighter in color. A simple magnetic separation was performed on some of the reduced catalysts using a bar magnet. The high manganese content catalysts could be separated into a magnetic (major) fraction and nonmagnetic (minor) fraction but the low manganese content catalysts could not be magnetically separated.

B. X-Ray Diffraction

X-Ray diffraction patterns for the reduced iron–manganese catalysts showed two phases, α-Fe and MnO (Fig. 2). In the low manganese content catalysts, the MnO peak was shifted from its true position toward the principal X-ray diffraction peak for FeO. The peak shift indicates a lattice contraction and is evidence of the inclusion of Fe(II)O in the Mn(II)O phase. The MnO XRD peak was also broader than that observed for bulk MnO.

C. BET Surface Area

The BET surface areas of reduced and passivated catalysts are shown in Fig. 3. Surface area values were between 5 and 8 m^2/g on a reduced weight basis. The low manganese and high manganese content catalysts had somewhat higher surface ar-

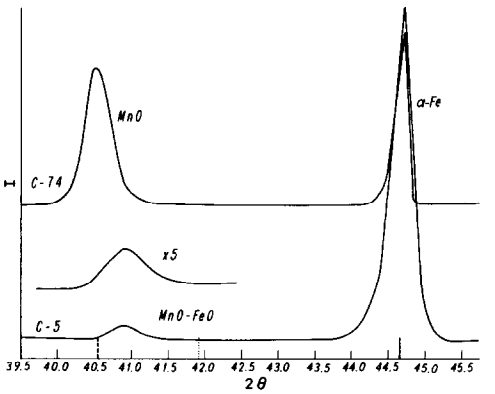

FIG. 2. XRD patterns of reduced iron–manganese catalysts C-5 and C-74. Markers: —, Fe; ---, MnO; ···, FeO.

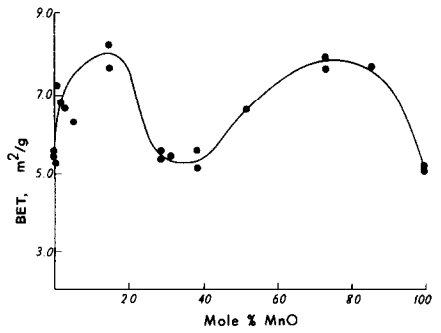

FIG. 3. BET surface areas of reduced iron–manganese catalysts.

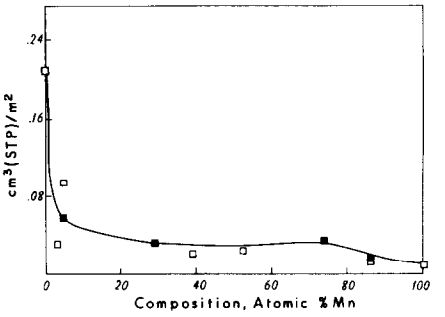

FIG. 4. Carbon monoxide chemisorption per unit surface area for iron–manganese catalysts. □, Room temperature; ■, −78°C.

eas than the intermediate or pure iron and pure manganese catalysts. The average particle diameter for the end members, assuming spherical particles, is 140 nm for the iron catalyst (C-0), and 220 nm for the manganese oxide catalyst (C-100).

D. Selective Chemisorption

The selective chemisorption experiments were aimed primarily at determining the specific surface areas of the iron and manganese oxide components of the catalysts. Carbon monoxide adsorbed readily on the pure iron catalyst but not on the pure manganese oxide catalyst. Carbon dioxide adsorbed on both catalysts but to a much greater degree on the pure manganese oxide catalyst. Oxygen interacted very strongly with iron and with manganese oxide. Hydrogen chemisorbed on the pure iron catalyst but the catalysts containing manganese exhibited very little hydrogen chemisorption.

Figure 4 displays the results of the carbon monoxide experiments. The adsorption is shown on a per unit surface area basis. The addition of manganese to the catalysts appreciably reduced the carbon monoxide chemisorption.

The oxygen and carbon dioxide chemisorption values obtained are shown in Fig. 5. Oxygen chemisorption generally decreased with increasing manganese content, rising somewhat for catalyst C-74. The oxygen chemisorption experiments are subject to some uncertainty because of the possibility of bulk oxidation of the iron phase. The carbon dioxide adsorption behavior is somewhat unusual. Though expected to increase, corresponding to the decrease in CO adsorption, it had a modest value for all the catalysts with less than 40% manganese and then generally increased with manganese content, reaching a maximum value on pure manganese oxide. Reproducibility for carbon dioxide adsorption was not especially good.

E. Electron Microscopy

The transmission electron microscope was used to examine individual catalyst particles in an attempt to distinguish the iron and manganese oxide phases. Individual iron particles were visible. They generally had a spherical shape and apparently varied from 50 to 400 nm, with an average

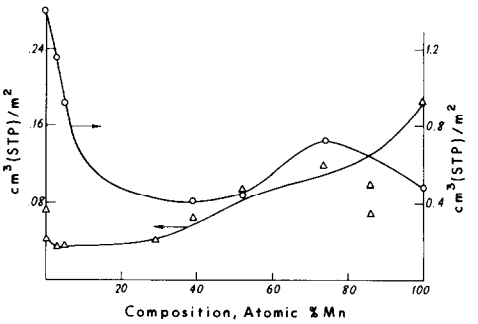

FIG. 5. Carbon dioxide and oxygen chemisorption per unit surface area for iron–manganese catalysts. ○, O_2; △, CO_2.

TABLE 2

Surface Concentrations of Reduced Catalysts by ESCA

Catalyst	$(N_{Mn}/N_{Fe})_{Bulk}$	I_{Mn}/I_{Fe}[b]	$(N_{Mn}/N_{Fe})^{c}_{Surf}$	Fe on surface atomic%
Mixture[a]	0.79	0.72	(0.79)	—
C-5	0.056	1.91	2.07	33
C-39	0.63	7.45	8.07	11
C-74	2.78	12.5	13.5	7

[a] Mixture of MnO + Fe.
[b] Peak ESCA intensity ratios for $3p_{1/2}$ peaks.
[c] Based on intensity ratio for mixture; $(N_{Mn}/N_{Fe})_{Surf} = (0.79/0.72)(I_{Mn}/I_{Fe})$.

particle size of about 200 nm in agreement with the average particle size calculated from the BET surface area. The particles were generally found in clusters and were rarely isolated.

The basic particles of the low manganese content catalysts appeared somewhat larger than for the pure iron catalyst, but the edge morphology was different from the smooth edges of the pure iron particles. The catalysts appeared to have protuberances from the basic particle body; their structure was finer than the bulk particle and presumably would add a substantial amount of surface area to the basic particle.

F. ESCA

The ESCA studies were used primarily to determine the relative surface concentrations of iron and manganese. Table 2 gives the Mn/Fe ESCA intensity ratios of the $3p_{1/2}$ peaks for several reduced catalysts. The intensity ratio of 0.72 for the mixture is in good agreement with a theoretical value of 0.67 calculated from photoelectron cross section values, viz. $(N_{Mn}/N_{Fe})_{bulk} \times$ (Fe/Mn) = 0.79(9.17/10.82). Therefore, the ratio 0.79/0.72 was applied to the intensity ratios to obtain the atomic Mn/Fe surface values. Compared to the bulk values, it is obvious that the surface is appreciably enriched in manganese for all the composite catalysts studied.

A comparison of the ESCA results with

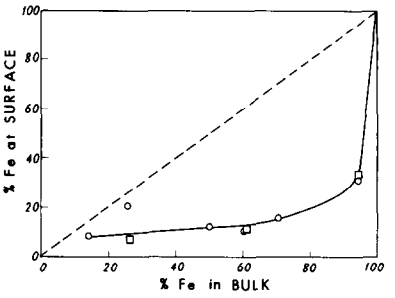

FIG. 6. Iron at surface from ESCA and CO chemisorption at −78°C. □, ESCA; ○, CO chemisorption.

results from the CO adsorption is shown in Fig. 6 in terms of %Fe on the surface versus %Fe in the bulk catalyst. Values of surface %Fe from CO chemisorption data were calculated by normalizing the adsorption uptakes to the BET area for the pure iron catalyst. This gave an adsorption stoichiometry of 2.9 Fe/CO, somewhat higher than the 2 Fe/CO quoted in the literature (*9*). The results of both techniques are in good agreement and show extensive surface enrichment in Mn for all catalysts.

G. Infrared Spectra

Catalysts C-0, C-3, and C-74 were examined by PAS-IR after exposure of the reduced catalysts to CO. Figure 7 shows the spectrum obtained after subtraction of the spectrum of the reduced catalyst. The presence of adsorbed CO (2013 and 2032 cm^{-1}) is noted. Results with the other two cata-

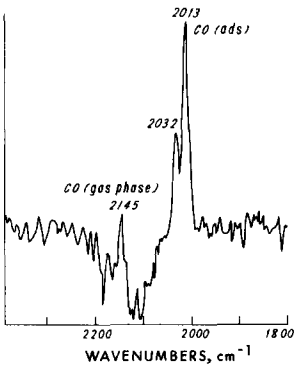

FIG. 7. Infrared photoacoustic difference spectra for CO adsorbed on catalyst C-0.

TABLE 3

TPD/TPR Results for Catalysts

Product	Catalyst	Step		
		CO/TPD 1	H_2/TPR 2	CO/TPR 3
CH_4	C-0	Nil	vs(325–500)	Nil
	C-5	Nil	l(400–500)	m(350–500)
	C-15	Nil	s(400–450)	vs(280–330)
	C-39	Nil	m(400–490)	s(250–500)
	C-74	Nil	s(400–500)	s(350–500)
	C-100	Nil	Nil	Nil
H_2O	C-0	Nil	m(270–370)	Nil
	C-5	Nil	m(250–500)	vl(250–500)
	C-15	Nil	m(410–500)	vs(400–500)
	C-39	Nil	s(450–500)	Nil
	C-74	Nil	vs(200–250) s(450–500)	vs(475–500)
	C-100	Nil	s(450–500)	Nil
CO	C-0	vs(50–100)	Nil	Nil
	C-5	s(50–100)	Nil	m(50–150) s(350–450)
	C-15	s(70–120) s(420–500)	Nil	vs(70–120)
	C-39	s(70–150) vs(470–500)	Nil	s(75–150)
	C-74	vs(50–100)	s(300–450)	m(80–150) s(400–500)
	C-100	Nil	vs(180–200)	Nil
CO_2	C-0	Nil	Nil	Nil
	C-5	vs(80–350)	Nil	Nil
	C-15	vs(170–350)	Nil	Nil
	C-39	vs(170–350)	vs(25–200)	Nil
	C-74	s(150–350)	s(50–200)	Nil
	C-100	Nil	vs(180–220)	Nil

Note. Values in parentheses are temperature ranges in °C. Relative peak heights: vs, very small; s, small; m, moderate; l, large; vl, very large.

lysts were negative, i.e., no adsorbed CO was detected. These results are in line with the drastic drop in CO adsorption (Fig. 4) when Mn is added. Either the PAS-IR technique was not sufficiently sensitive to detect the lower adsorption levels, or the CO was more weakly held and removed during the brief evacuation used after adsorption.

H. Temperature-Programmed Desorption/Reduction

The temperature-programmed desorption and temperature-programmed reduction studies provided qualitative information on the strength of adsorption and also provided a measure of surface reactivity and reaction product selectivity. The results of these experiments on six catalysts are summarized in Table 3. The temperature ranges of the main peaks are given in parentheses; peak maxima were usually about in the middle of the range. A typical profile for the TPR of catalyst C-5 is shown in Fig. 8.

In general, carbon monoxide adsorption occurred to varying degrees with all the catalysts containing iron. During TPD (Step 1) some, but not all, of the carbon monoxide desorbed. Small amounts of carbon dioxide were also produced in the manganese-containing catalysts during Step 1. Subsequent TPR (Step 2) formed CH_4 and H_2O. Similar results were obtained during TPR of adsorbed carbon monoxide on the catalysts (Step 3). Pure MnO did not adsorb carbon monoxide.

The temperature of water evolution in Step 2 seemed to increase with increasing MnO content in the catalysts. Except for catalyst C-5, very little water was detected during Step 3. However, analysis of water evolution is hampered by possible adsorption in the lines leading to the mass spectrometer.

The evolution of carbon monoxide generally occurred at low temperatures (50–100°C) and this weakly adsorbed carbon monoxide was observed on all catalysts except pure MnO. In addition, some catalysts showed a very small evolution of carbon monoxide at high temperatures.

Carbon dioxide evolution was usually

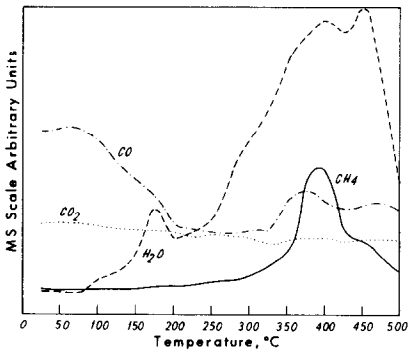

FIG. 8. TPR of preadsorbed CO on catalyst C-5 (Step 3).

small but increased somewhat for catalysts heavily promoted with MnO. Step 1 showed the most consistent carbon dioxide evolution. In the presence of hydrogen (Steps 2 and 3) carbon dioxide evolution was generally eliminated. Overall, the MnO catalyst was inactive with respect to the TPD/TPR experiments.

DISCUSSION

A. Catalyst Reduction

The reduction process was not extensively studied, but the weight loss curves showed that 98% of the final weight could be achieved within an hour with the conditions employed. Colombo *et al.* (*10*) proposed a stepwise process for iron–oxide reduction at temperatures below 400°C, viz., $Fe_2O_3 \rightarrow Fe_3O_4 \rightarrow Fe_{3+w}O_4 \rightarrow Fe$. The migration of iron cations to the reaction interface was the proposed reduction mechanism. Other researchers (*11–13*) also concluded that iron cations and not oxygen anions migrated during wustite (FeO) reduction. In the reduction of the iron–manganese oven-dried catalysts, a clear stepwise reduction process was not seen. However, it is important to note that at least two oxide phases of iron and manganese are considered to form solid solutions: Fe_3O_4–Mn_3O_4 and FeO–MnO. In a stepwise reduction, the segregation of α-Fe from the MnO–FeO phase would probably be the final step. The proposed iron cation migration mechanism is consistent with the apparent partial covering of the iron particles by manganese oxide for the low manganese content catalysts (see latter). The difficult to reduce oxide evidently remained relatively immobile on the surface during reduction by virtue of combination with the MnO phase.

After reduction and subsequent air passivation at room temperature, the low-manganese-content catalysts showed evidence of iron(II) oxide inclusion in the manganese oxide phase, as shown in the X-ray diffraction patterns. An almost linear shift in the lattice constant with composition has been reported for FeO–MnO solid solution (*14*). The iron content in the manganese oxide phase varied, but was usually less than 30% and generally decreased as manganese content in the catalysts increased; the high manganese catalysts showed little evidence of unreduced iron in the manganese oxide phase. Thermodynamically, the reduction of the FeO in the MnO–FeO phase would be expected to be difficult (*15*).

B. Structure of Reduced Catalysts

The structure of the reduced catalysts provides a starting point for the discussion of other aspects of the catalysts, such as their carburization, activity, and selectivity characteristics discussed in the following paper (*16*). The catalysts are roughly categorized by their manganese content. Two models of the catalysts will be discussed here: a low manganese content model and a high manganese content model. The models are based on the combined results of the XRD, surface area, selective chemisorption, magnetic separation, and ESCA experiments. The electron microscopy experiments provide further general substantiation.

1. Low manganese model. From the TEM micrographs, it is evident that the low manganese catalysts (Mn < 30%) are composed of assemblages of particles. The general shape of the basic particle is spherical. The model is based on the structural effect of manganese oxide on the average iron particle. A small addition of manganese increased the BET surface area of the catalysts (Fig. 3), but decreased the carbon monoxide chemisorption (Fig. 4). Further, the ESCA results showed a surface enrichment in manganese. These facts indicate that the manganese oxide phase covers a substantial portion of the basic iron particle, resulting in loss in iron surface area and at the same time an increase in the overall surface area. Considering a basic iron particle size, and knowing the density of the iron and manganese oxide phases, a model of an

TABLE 4

Phase Analysis for Reduced Catalyst C-5

	Fe	MnO
Composition		
mole%	94.7	5.3
wt%	93.2	6.7
Specific surface area, m^2/g cat	1.7	4.6
Average particle sizes		
Spherical diameter, nm	140	
Height of platelet, nm		3.6
Width of platelet, nm		42.7
Equivalent platelet diameter, nm		18.7[a]
X-Ray analysis		
Average diameter, nm		18
FeO in FeO–MnO, mole fraction		0.25

[a] Equivalent dimension of MnO cubes = (height × $width^2)^{1/3}$.

average iron–manganese oxide particle can be derived from the BET and selective chemisorption data, assuming that no manganese oxide is occluded in the iron particle. In a study of ammonia synthesis catalysts, Pernicone *et al.* (*17*) found little evidence for insertion of MnO-containing clusters in the lattice of Fe. The rapid loss of carbon monoxide adsorption capability with small amounts of manganese oxide also supports the idea of little occlusion of this phase.

The low manganese model envisions flat platelets or disks of manganese oxide partially covering the basic iron particles, which are assumed to be spherical and have the same average size as found in the pure iron catalysts (140 nm). For calculation purposes, the manganese oxide platelets are assumed to have a square geometry of dimension w and height h. Table 4 summarizes the results obtained from this model employing the BET surface area and carbon monoxide chemisorption data for catalyst C-5. According to this model, there are about 20 manganese oxide platelets per iron particle and about 60% of the iron surface is covered by manganese oxide. The average manganese oxide particle size estimated from X-ray diffraction line broadening agrees well with the calculated value of an equivalent cubic particle.

The TEM micrographs of catalysts C-5 showed a different edge structure than the pure-iron catalyst, C-0. Although the composition of these protuberances was not established, they presumably were the manganese oxide phase. These structures did not appear exactly plate-like, but they would increase BET surface area.

2. High manganese model. The high manganese model of the reduced catalysts is an attempt to unify various experimental observations and the model presently remains tentative. This model is proposed for catalysts containing 50–90 mole% manganese oxide and is based on a composition distribution of iron and manganese in the fundamental catalyst particles; that is, the basic catalyst particles vary in the relative amount of iron and manganese present, some rich in manganese oxide, some rich in iron. The iron-rich catalyst particles are considered as heavily manganese oxide covered iron particles described in basic structure by the low manganese model. In some cases, the manganese oxide phase may possibly encapsulate the iron. The manganese-rich catalysts particles consist of relatively small iron crystallites supported on manganese oxide. These particles are best visualized as similar to a very high manganese oxide content catalyst in which the manganese oxide essentially performs the role of a traditional oxide support. Therefore, the high manganese model becomes, to a degree, the expected result of an intimate mixture of low and high manganese catalysts. The relative population of the two components would vary, of course, with the mean catalyst composition.

The X-ray diffraction data is generally consistent with this model. Little X-ray line broadening was observed for the iron phases of the high manganese content catalysts. Evidently, a substantial portion of the iron remained as fairly large particles surrounded by manganese oxide. The small amount of supported iron crystallites did

not noticeably affect the diffraction spectra. The manganese oxide phase also showed little evidence of broadening or the presence of FeO. Presumably, during reduction, much of the iron congregated into relatively large iron particles but a small amount of iron, unable to reach any large particles, remained in the excess manganese oxide phase and formed relatively small iron crystallites on the surface.

The high manganese catalysts could be magnetically separated into two fractions. This indicates that some sort of compositional segregation occurred in these catalysts. Usually, the less magnetic fraction of the catalyst was noticeably lighter in color than the magnetic fraction. Though its composition was not determined, this fraction was undoubtedly rich in manganese oxide. A simple comparison of the two fractions using X-ray diffraction was performed and the peak height ratio for iron in the less magnetic versus the magnetic fraction was found to be 0.06. The manganese-rich fraction would be expected to contain a relatively greater number of small iron crystallites than the magnetic fraction. It is difficult to estimate the size or morphology of the proposed small iron crystallites; however, they would be expected to be less than 2 nm. It is interesting to note that less than 1% of the iron present in catalyst C-74 could give the measured carbon monoxide adsorption value if distributed as very small iron particles; so much of the iron could remain relatively occluded. The apparent small size may contribute to the difficulty of seeing the iron particles in the transmission electron micrographs.

C. Catalyst Interaction with Adsorbed Species

Carbon monoxide was found to adsorb on all catalysts, though the adsorption on pure manganese oxide was small. The presence of manganese oxide lessened substantially the amount of carbon monoxide chemisorbed. The decrease in carbon monoxide adsorption, however, is ascribed to the structure of the catalysts and not to a chemical promoter effect that lessened chemisorption without decreasing effective iron surface area, though such an effect is a possibility. Carbon monoxide chemisorption was, therefore, used to calculate effective iron surface area.

The interaction of carbon monoxide with the iron–manganese catalysts was investigated using TPD/TPR. The temperature-programmed desorption of preadsorbed carbon monoxide in helium (Step 1) gave relatively little desorption. Usually a small peak was observed below 100°C and occasionally, a very high temperature desorption peak (420°C) was observed. The low-temperature desorption indicates weak associatively adsorbed carbon monoxide while the high-temperature peak probably resulted from the recombination and desorption of dissociatively adsorbed carbon monoxide. This general behavior is consistent with the carbon monoxide TPD results observed by Amenomiya and Pleizier (*18*) using an ammonia synthesis catalyst. For the iron–manganese catalysts, a small amount of carbon dioxide was also found to desorb during Step 1 at lower temperature than the high-temperature carbon monoxide desorption. This is probably due to a disproportionation of the adsorbed carbon monoxide.

Both strongly adsorbed carbon monoxide (presumably dissociated) and residual carbon from carbon monoxide disproportionation remain on the surface after TPD. The results of hydrogen TPR of the catalysts (Step 2) show clearly that this is the case. The principle products are water and methane, with some carbon dioxide formation for some heavily manganese-promoted catalysts. Generally, water formation occurred at lower temperatures than methane formation. After the helium TPD, any adsorbed carbon monoxide would almost certainly be dissociated and the formation of water and methane at different temperatures supports this view. The formation or decomposition of an "enol" (HCOH) inter-

mediate as the slow step of reaction presumably would lead to simultaneous release of water and methane.

The temperature-programmed reaction of preadsorbed carbon monoxide with hydrogen (Step 3) provided information about the reactivity of freshly adsorbed carbon monoxide. Comparing Step 3 with Step 2, methane formation was found to occur at somewhat lower temperatures, while water formation occurred at about the same temperature. Evidently, even with the high-temperature treatment of the catalyst in Step 1, oxygen may be removed at similar temperatures. In the CO/TPR (Step 3), the surface carbon formed from the dissociative adsorption of carbon monoxide is more reactive and easier to hydrogenate than the carbon after TPD (Step 2). No carbon dioxide was formed during Step 3, but some carbon monoxide escaped unreacted, especially at lower temperatures. Comparing Steps 2 and 3 for carbon monoxide evolution, once carbon monoxide is dissociatively adsorbed after Step 1, when reacted with hydrogen in Step 2, the oxygen and carbon atoms leave the surface mainly as hydrogen-containing products (i.e., little carbon dioxide or carbon monoxide). As seen in Step 3, if some weakly bound carbon monoxide is present ($T_m < 150$°C), then it may leave the surface without reacting even in hydrogen. Again in Step 3, the formation of water and methane commence and peak at independent temperatures, implying the dissociation of carbon monoxide has already occurred before reaction.

The presence of manganese oxide seemed to promote dissociative adsorption of carbon monoxide and significantly reduce hydrogen chemisorption. A possible explanation is based on the supposition that manganese oxide is a strong electron donor. Manganese oxide alone exhibits surface basicity (*19*) as evidenced by carbon dioxide adsorption. However, manganese oxide may have a greater effect on iron than that simply inferred from carbon dioxide adsorption. Dry *et al.* (*20*) observed that K_2O increased the heat of carbon monoxide adsorption at low coverages while it decreased the initial heats of hydrogen adsorption. More recently, Broden *et al.* (*21*) studied carbon monoxide adsorption on potassium-promoted iron. With the potassium-promoted iron, they found the binding energy for carbon monoxide adsorbed at room temperature increased, as well as an increased probability of the adsorbed carbon monoxide to dissociate upon heating. These potassium promoters are thought to donate electrons to the iron, increasing its electron density.

Dry *et al.* (*20*) argued that carbon monoxide tends to accept electrons from iron upon adsorption; thus, electron-donating promoters would increase the strength of the iron-to-carbon bond. Conversely, since hydrogen can donate electrons on adsorption (*22*), electron-donating promoters could tend to weaken the iron–hydrogen bond. Presumably iron, in the presence of a very strong electron donor, could be expected to so weaken the carbon–oxygen bond in carbon monoxide that dissociative adsorption occurs rapidly while hydrogen chemisorption would be significantly reduced. It is possible that manganese oxide performs this function. A very recent study (*23*), however, found the heat of hydrogen chemisorption to increase slightly for potassium-promoted Fe(110) and Fe(111) over that for the unpromoted crystal faces. Therefore, presently it is not clear why the manganese-promoted iron catalysts had such low values of hydrogen chemisorption.

CONCLUSIONS

1. The reduced iron–manganese catalysts consisted of two principal phases: α-Fe and MnO. Evidence for some inclusion of FeO in the MnO phase was found for low manganese content catalysts. Also, some evidence was deduced for a manganese oxide-rich and iron-rich segregation in the high manganese content catalysts. The reduced catalysts consisted of assemblages of parti-

cles, generally 100–300 nm in diameter. In the low manganese catalysts, a manganese-rich oxide phase partially covers the basic iron particle. In the high manganese catalysts, apparently many of the larger iron particles are encapsulated by manganese oxide, but some iron is believed to be present as small crystallites supported on the manganese oxide phase.

2. Temperature-programmed desorption and infrared photoacoustic spectroscopy of preadsorbed carbon monoxide indicate the presence of some weak, probably associatively bound, carbon monoxide on the reduced catalysts. Temperature-programmed reaction studies show that appreciable dissociation also occurred during adsorption of carbon monoxide.

ACKNOWLEDGMENTS

We gratefully acknowledge Mr. J. A. Jiang of the Chemistry Department for obtaining the PAS data. This research was supported by the Department of Energy and the State of Utah.

REFERENCES

1. Bussemeier, B., Frohning, C. D., and Cornils, B., *Hydrocarbon Process.* **55**(11), 101 (1976).
2. Kobel, H., Ralek, M., and Tillmitz, K. O., "Proceedings, 15th Intersoc. Energy Conv. Eng. Conf., Soc. of Automotive Eng., San Diego," p. 482 (1978).
3. Yang, C. H., Ph.D. dissertation, University of Utah, Salt Lake City, Utah, 1979.
4. Tsai, Y. S., M.S. thesis, University of Utah, Salt Lake City, Utah, 1980.
5. Van Dijk, W. L., Niemantsverdriet, J. W., Van Der Kraan, A. M., and Van Der Baan, H. S., *Appl. Catal.* **2,** 273 (1982).
6. Deckwer, W. D., Serpemen, Y., Ralek, M., and Schmidt, B. *Ind. Eng. Chem. Proc. Des. Dev.* **21,** 222 (1982).
7. Lloyd, L. B., Riseman, S. M., Burnham, R. K., and Eyring, E. M., *Rev. Sci. Instrum.* **51,** 1488 (1980).
8. Jensen, K. B., Ph.D. dissertation, University of Utah, Salt Lake City, Utah, 1982.
9. Boudart, M., Delbouille, A., Dumesic, J. A., Khammouma, S., and Topsøe, H., *J. Catal.* **37,** 486 (1975).
10. Colombo, U., Gazzarrini, F., and Lanzavecchia, G., *Mater. Sci. Eng.* **2,** 125 (1967).
11. Landler, P. F. J., and Komerek, K. L., *Trans. Metall. Soc. AIME* **236,** 138 (1966).
12. Edstroem, J. O., and Bitsianes, G., *Trans. Metall. Soc. AIME* **203,** 760 (1955).
13. Davies, M. H., Simnad, M. I., and Birchenad, C. E., *Trans. Metall. Soc. AIME* **191,** 889 (1951).
14. Foster, P. K., and Welch, A. J. E., *Trans. Faraday Soc.* **1956,** 1626 (1956).
15. Foster, P. K., and Welch, A. J. E., *Trans. Faraday Soc.* **1956,** 1636 (1956).
16. Jensen, K. B., and Massoth, F. E., *J. Catal.* **92,** 109 (1985).
17. Pernicone, N., Fagherazzi, G., Galante, F., Barbassi, R., Lazzerin, F., and Mattera, A., *in* "Proceedings, 5th International Congress on Catalysis, Palm Beach, 1972 (J. W. Hightower, Ed.), p. 1241. North-Holland, Amsterdam, 1973.
18. Amenomiya, Y., and Pleizier, G., *J. Catal.* **28,** 442 (1973).
19. Dry, M. E., and Oosthuizen, G. J., *J. Catal.* **11,** 18 (1968).
20. Dry, M. E., Shingles, T., Boshoff, L. J., and Oosthuizen, G. J., *J. Catal.* **15,** 190 (1969).
21. Broden, G., Gafner, G., and Bonzel, H. P., *Surf. Sci.* **84,** 295 (1979).
22. Artyukh, Y. N., Lunev, N. K., and Rusov, M. T., *Kinet. Katal.* **13,** 741 (1972).
23. Ertl, G., Lee, S. B., and Weiss, M., *Surf. Sci.* **111,** L711 (1981).